49th AIAA/ASME/ASCE/AHS/ASC Structures, Structural Dynamics, and Materials Conference
 16t
7 - 10 April 2008, Schaumburg, IL

AIAA 2008-2332

Reduced-Order Model Construction Procedure for Robust Mistuning Identification of Blisks

Andrew C. Madden*, Matthew P. Castanier†, and Bogdan I. Epureanu‡
University of Michigan, Ann Arbor, Michigan 48109-2125

The reduced-order modeling of integrally bladed disks (blisks) for predicting the mistuned vibration response has been well studied and understood. For solving a direct vibration problem, adding modes to the modeling basis improves the accuracy of the reduced-order model (ROM) with respect to the parent finite element model. In contrast, when solving an inverse problem for system identification, adding modes to the ROM while using the same measurements may actually reduce its accuracy. This is especially true for solving inverse problems related to identification of blade mistuning parameters, because the characteristics of the selected system modes for the ROM may not match well the assumptions used in the mistuning modeling approach. In this work, a procedure is introduced for constructing a ROM referred to as the inverse ROM (IROM) that is well suited for solving the mistuning identification inverse problem. First, a quantitative metric is defined to characterize and rank the tuned system modes with respect to their suitability for constructing IROMs. Then, the direct problem is solved using a larger direct ROM (or DROM) with prescribed mistuning in order to interrogate and validate the performance of various IROMs as modes are added. This enables the automated construction of suitable IROMs and improves the overall accuracy and robustness of mistuning identification.

I. Introduction

Small deviations among the structural properties of the blades in an otherwise cyclically symmetric bladed disk can result in significant changes to the forced response behavior of the structure. These small blade-to-blade deviations, called mistuning, can arise due to reasons such as manufacturing tolerances, general wear over the life cycle, and damage. Mistuning has been shown to increase the forced response for a bladed disk which can be a concern for high cycle fatigue.[1] Furthermore, due to mistuning, the cyclic symmetry of the system is destroyed along with the possibility of using efficient cyclic symmetry solvers to predict the vibration response. As a result, a large body of research exists on constructing reduced-order models (ROMs) of mistuned bladed disk vibration based on tuned system and/or component modes.[2–8]

With capabilities to model and study mistuning of bladed disks in place, several recent research efforts have focused on the identification of the mistuning parameters using experimentally measured system response data. Such system-based mistuning identification procedures are essential for the case of bladed disks manufactured as a single piece (called blisks), because the blades cannot be separated from the disk and tested individually. Mistuning identification results can also be used for evaluating manufacturing processes and identifying wear and damage during maintenance checks. Work in this area has ranged from simple lumped parameter models[9,10] to more involved reduced-order modeling techniques.[11–21] Judge *et al.*[11] found that the identified mistuning parameters were sensitive to errors in the finite element model (FEM) or measurement data. Later, Lim *et al.*[19] found that the identification results showed especially high sensitivity to errors in the tuned system eigenvalues for the modes used in the ROM.

Sensitivity to the FEM and measurement data and their use in the ROM is the subject of this work. Pichot *et al.*[22] recently presented a mistuning identification procedure where the measured modes were filtered using the Best Achievable Eigenvectors[23] approach in order to reduce the errors that occur in the

*Graduate Student Research Assistant, Department of Mechanical Engineering. Student Member of AIAA.
†Associate Research Scientist, Department of Mechanical Engineering. Senior Member of AIAA.
‡Associate Professor, Department of Mechanical Engineering. Member of AIAA.

measurement data. The work presented here considers the component mode mistuning (CMM) approach to mistuning identification[19,20] and explores ways to enhance the procedure given the modeling technique and the limitations of the experimental portion of the approach. In order to select tuned system normal modes that will best fit the assumptions of the CMM approach, a parameter based on cantilevered blade participation factors and blade-disk interface motion is introduced. Using modes selected as favorable for the ROM according to this parameter can result in increased accuracy for the mistuning identification procedure. In this work, a procedure is introduced for constructing a ROM referred to as an inverse ROM (or IROM) that is well suited for solving the mistuning identification inverse problem. Also, representing the mode shapes using a limited number of measured degrees of freedom (DOF) is accounted for because of the likely possibility that the corresponding modal matrix is rank deficient. Limitations for the types of mode shapes that can be used are discussed. Finally, a method is presented that can be used to determine a suitable IROM size. By using an assumed mistuning pattern, a forward problem can be formulated and used to generate surrogate data, which are then used to identify the mistuning in the inverse problem and thus assess the accuracy of the IROM.

II. Theory

A. Background: Mistuning Identification and Model Updating Based on the CMM Method

Consider the equations of motion for an elastic structure expressed as

$$\mathbf{M}\ddot{\mathbf{X}} + \mathbf{K}\mathbf{X} + \mathbf{F}_{sd} = \mathbf{F}_{ext}, \tag{1}$$

where $\mathbf{M}$ and $\mathbf{K}$ are the usual mass and stiffness matrices, $\mathbf{F}_{sd}$ denotes the force caused by structural damping, and $\mathbf{F}_{ext}$ is the external forcing. Let the external excitation be $\mathbf{F}_{ext} = \mathbf{f}e^{j\omega t}$ and assume that $\mathbf{X} = \mathbf{x}e^{j\omega t}$. Hence, the structural damping forces are $\mathbf{F}_{sd} = j\gamma\mathbf{K}\mathbf{x}e^{j\omega t}$, where γ is the structural damping factor. Substituting into Eq. 1, one obtains

$$-\omega^2\mathbf{M}\mathbf{x} + (1 + j\gamma)\,\mathbf{K}\mathbf{x} = \mathbf{f}. \tag{2}$$

If the structure of interest is a mistuned bladed disk or blisk, the CMM method developed by Lim *et al.*[7,8] can be implemented. The CMM procedure treats the tuned system as a free-interface component and the mistuned portions of the system are treated as fixed-interface components. Using component mode synthesis (CMS),[24,25] the following is obtained for the tuned system

$$\begin{aligned}
\mu^s &= \begin{bmatrix} \mathbf{I} & {\boldsymbol{\Phi}^s}^T\mathbf{M}^s\boldsymbol{\Psi}^s \\ {\boldsymbol{\Psi}^s}^T\mathbf{M}^s\boldsymbol{\Phi}^s & {\boldsymbol{\Psi}^s}^T\mathbf{M}^s\boldsymbol{\Psi}^s \end{bmatrix}, \\
\kappa^s &= \begin{bmatrix} \boldsymbol{\Lambda}^s & {\boldsymbol{\Phi}^s}^T\mathbf{K}^s\boldsymbol{\Psi}^s \\ {\boldsymbol{\Psi}^s}^T\mathbf{K}^s\boldsymbol{\Phi}^s & \boldsymbol{\Psi}^s_A \end{bmatrix}, \\
\mathbf{x}^s &= \begin{bmatrix} \boldsymbol{\Phi}^s_O & \boldsymbol{\Phi}^s_O \\ \boldsymbol{\Phi}^s_A & \boldsymbol{\Phi}^s_A \end{bmatrix} \begin{Bmatrix} \mathbf{p}^s_\Phi \\ \mathbf{p}^s_\Psi \end{Bmatrix},
\end{aligned} \tag{3}$$

where μ^s and κ^s are reduced mass and stiffness matrices of the tuned system, $\mathbf{p}^s_\Phi$ and $\mathbf{p}^s_\Psi$ are modal coordinates, O and A refer to omitted and active (where mistuning exists) DOF, respectively, and s denotes the tuned system. Also, $\boldsymbol{\Phi}^s$ and $\boldsymbol{\Psi}^s$ are the tuned system normal modes and constraint modes corresponding to mistuned DOF, respectively, while $\mathbf{M}^s$ and $\mathbf{K}^s$ are the tuned mass and stiffness matrices. The mistuned portion is represented only as constraint modes because all of the mistuning DOF are considered interface DOF so that

$$\begin{aligned}
\mu^\delta &= \mathbf{M}^\delta, \\
\kappa^\delta &= \mathbf{K}^\delta, \\
\mathbf{x}^\delta &= \mathbf{x}^\delta_\Psi.
\end{aligned} \tag{4}$$

Here, δ denotes the mistuned portion of the system, and Ψ indicates the modal coordinates associated with the interface DOF. The CMS synthesized equations follow as

$$\begin{aligned}
\mu_{CMS}^{syn} &= \mu^s + \begin{bmatrix} \boldsymbol{\Phi}_A^{s^T}\mathbf{M}^\delta\boldsymbol{\Phi}_A^s & \boldsymbol{\Phi}_A^{s^T}\mathbf{M}^\delta\boldsymbol{\Psi}_A^s \\ \boldsymbol{\Psi}_A^{s^T}\mathbf{M}^\delta\boldsymbol{\Phi}_A^s & \boldsymbol{\Psi}_A^{s^T}\mathbf{M}^\delta\boldsymbol{\Psi}_A^s \end{bmatrix}, \\
\kappa_{CMS}^{syn} &= \kappa^s + \begin{bmatrix} \boldsymbol{\Phi}_A^{s^T}\mathbf{K}^\delta\boldsymbol{\Phi}_A^s & \boldsymbol{\Phi}_A^{s^T}\mathbf{K}^\delta\boldsymbol{\Psi}_A^s \\ \boldsymbol{\Psi}_A^{s^T}\mathbf{K}^\delta\boldsymbol{\Phi}_A^s & \boldsymbol{\Psi}_A^{s^T}\mathbf{K}^\delta\boldsymbol{\Psi}_A^s \end{bmatrix}, \\
\mathbf{p}_{CMS}^{syn} &= \begin{Bmatrix} \mathbf{p}_\Phi^s \\ \mathbf{p}_\Psi^s \end{Bmatrix}.
\end{aligned} \tag{5}$$

Next, one assumes that the tuned system modes of interest are in a small frequency range. According to work by Yang and Griffin,[5,26] this suggests that the mistuned normal modes are also in a small frequency band and therefore can be represented by a small set of tuned system normal modes in the frequency range of interest. This implies that other normal modes and static modes can be ignored. Equation 5 leads to a reduced order forumulation expressed as

$$\begin{aligned}
\mu^{syn} &= \mathbf{I} + \boldsymbol{\Phi}_A^{s^T}\mathbf{M}^\delta\boldsymbol{\Phi}_A^s, \\
\kappa^{syn} &= \boldsymbol{\Lambda}^s + \boldsymbol{\Phi}_A^{s^T}\mathbf{K}^\delta\boldsymbol{\Phi}_A^s, \\
\mathbf{p}^{syn} &= \mathbf{p}_\Phi^s = \mathbf{p}.
\end{aligned} \tag{6}$$

Combining Eq. 2 with Eq. 6 and neglecting mass mistuning ($\mathbf{M}^\delta$) yields

$$-\omega^2\mathbf{p} + (1+j\gamma)\left[\boldsymbol{\Lambda}^s + \boldsymbol{\Phi}^{s^T}\mathbf{K}^\delta\boldsymbol{\Phi}^s\right]\mathbf{p} = \boldsymbol{\Phi}^{s^T}\mathbf{f}. \tag{7}$$

In Lim *et al.*[19,27], an additional term was added to this equation to account for the difference between the parent tuned system FEM and the virtual tuned system of an actual bladed disk, which was called the cyclic modeling error. This term allows the tuned FEM to be updated using the mistuning procedure in order to more closely match the tuned portion of the actual bladed disk being examined. Adding this term to Eq. 7, one obtains

$$\begin{aligned}
-\omega^2\mathbf{p} + (1+j\gamma)\left[\boldsymbol{\Lambda}^s + \boldsymbol{\Phi}^{s^T}\left(\mathbf{K}^{\delta,s} + \mathbf{K}^\delta\right)\boldsymbol{\Phi}^{\mathbf{s}}\right]\mathbf{p} &= \boldsymbol{\Phi}^{s^T}\mathbf{f}, \\
-\omega^2\mathbf{p} + (1+j\gamma)\left[\boldsymbol{\Lambda}^s + \boldsymbol{\Lambda}^{\delta,s} + \boldsymbol{\Phi}^{s^T}\mathbf{K}^\delta\boldsymbol{\Phi}^s\right]\mathbf{p} &= \mathbf{f}^s,
\end{aligned} \tag{8}$$

where $\boldsymbol{\Lambda}^{\delta,\mathbf{s}}$ is the matrix of deviations of the actual tuned system eigenvalues from those of the FEM, and $\mathbf{K}^{\delta,\mathbf{s}}$ is the deviation of the mistuned system stiffness matrix from that of the actual tuned system. The term $\boldsymbol{\Phi}^{s^T}\mathbf{K}^\delta\boldsymbol{\Phi}^s$ corresponds to the mistuned portion of the stiffness matrix. It should be noted that this term is not decoupled/diagonalized using this modal decomposition. In order to decouple this portion of the equation and to further reduce the model, the blade portion of the system normal modes, $\boldsymbol{\Phi}^s$ is represented using a basis of cantilevered blade normal modes denoted by $\boldsymbol{\Phi}^{cb}$. Furthermore, in these coordinates, the off-diagonal terms are considered negligible[27]. Assuming that $\boldsymbol{\Phi}^s = \boldsymbol{\Phi}^{cb}\mathbf{q}$, Eq. 8 can be written as

$$\begin{aligned}
-\omega^2\mathbf{p} + (1+j\gamma)\left[\boldsymbol{\Lambda}^s + \boldsymbol{\Lambda}^{\delta,s} + \mathbf{q}^T\boldsymbol{\Phi}^{cb^T}\mathbf{K}^\delta\boldsymbol{\Phi}^{cb}\mathbf{q}\right]\mathbf{p} &= \mathbf{f}^s, \\
-\omega^2\mathbf{p} + (1+j\gamma)\left[\boldsymbol{\Lambda}^s + \boldsymbol{\Lambda}^{\delta,s} + \mathbf{q}^{\mathrm{T}}\boldsymbol{\Lambda}^{\delta,cb}\mathbf{q}\right]\mathbf{p} &= \mathbf{f}^s.
\end{aligned} \tag{9}$$

Eq. 9 can be rearranged as follows

$$(1+j\gamma)\left[\boldsymbol{\Lambda}^{\delta,s} + \mathbf{q}^T\boldsymbol{\Lambda}^{\delta,cb}\mathbf{q}\right]\mathbf{p} = \mathbf{f}^s + \omega^2\mathbf{p} - (1+j\gamma)\boldsymbol{\Lambda}^s,$$

or

$$(1+j\gamma)\left[\boldsymbol{\Lambda}^s\left(\boldsymbol{\Lambda}^{s^{-1}}\boldsymbol{\Lambda}^{\delta,s}\right) + \mathbf{q}^T\boldsymbol{\Lambda}^{cb}\left(\boldsymbol{\Lambda}^{cb^{-1}}\boldsymbol{\Lambda}^{\delta,cb}\right)\mathbf{q}\right]\mathbf{p} = \mathbf{f}^s + \omega^2\mathbf{p} - (1+j\gamma)\boldsymbol{\Lambda}^s. \tag{10}$$

Since $\mathbf{p}$ is a complex quantity, it can be written as $\mathbf{p} = \mathbf{p}_r + j\mathbf{p}_i$. Substituting this into Eq. 10 and using $(1+j\gamma)(\mathbf{p}_r + j\mathbf{p}_i) = (\mathbf{p}_r - \gamma\mathbf{p}_i) + j(\mathbf{p}_i + \gamma\mathbf{p}_r)$ yields

$$\begin{aligned}
\left[\boldsymbol{\Lambda}^s\left(\boldsymbol{\Lambda}^{s^{-1}}\boldsymbol{\Lambda}^{\delta,s}\right) + \mathbf{q}^T\boldsymbol{\Lambda}^{cb}\left(\boldsymbol{\Lambda}^{cb^{-1}}\boldsymbol{\Lambda}^{\delta,cb}\right)\mathbf{q}\right]\left[(\mathbf{p}_r - \gamma\mathbf{p}_i) + j(\mathbf{p}_i + \gamma\mathbf{p}_r)\right] = \\
\mathbf{f}^s + \omega^2(\mathbf{p}_r + j\mathbf{p}_i) - \boldsymbol{\Lambda}^s\left[(\mathbf{p}_r - \gamma\mathbf{p}_i) + j(\mathbf{p}_i + \gamma\mathbf{p}_r)\right].
\end{aligned} \tag{11}$$

Eq. 11 can be split into two equations corresponding to real and imaginary parts as

$$\begin{aligned}
\boldsymbol{\Lambda}^s \left(\boldsymbol{\Lambda}^{s^{-1}} \boldsymbol{\Lambda}^{\delta,s}\right) (\mathbf{p}_r - \gamma \mathbf{p}_i) + \mathbf{q}^T \boldsymbol{\Lambda}^{cb} \left(\boldsymbol{\Lambda}^{cb^{-1}} \boldsymbol{\Lambda}^{\delta,cb}\right) \mathbf{q} (\mathbf{p}_r - \gamma \mathbf{p}_i) &= \mathbf{f}^s + \omega^2 \mathbf{p}_r - \boldsymbol{\Lambda}^s (\mathbf{p}_r - \gamma \mathbf{p}_i), \\
\underbrace{\boldsymbol{\Lambda}^s}_{\mathbf{a}_{c1}} \left(\boldsymbol{\Lambda}^{s^{-1}} \boldsymbol{\Lambda}^{\delta,s}\right) \underbrace{(\mathbf{p}_i + \gamma \mathbf{p}_r)}_{\mathbf{a}_{c2}} + \underbrace{\mathbf{q}^T \boldsymbol{\Lambda}^{cb}}_{\mathbf{a}_{s1}} \left(\boldsymbol{\Lambda}^{cb^{-1}} \boldsymbol{\Lambda}^{\delta,cb}\right) \underbrace{\mathbf{q} (\mathbf{p}_i + \gamma \mathbf{p}_r)}_{\mathbf{a}_{s2}} &= \underbrace{\omega^2 \mathbf{p}_i - \boldsymbol{\Lambda}^s (\mathbf{p}_i + \gamma \mathbf{p}_r)}_{\mathbf{b}}.
\end{aligned} \tag{12}$$

The diagonal matrices associated with quantities to be identified are organized into column vectors and the rest of the equation is reshaped accordingly. The final matrix equation is represented by

$$\begin{bmatrix} \mathbf{A}_c & \mathbf{A}_s \end{bmatrix} \begin{bmatrix} \mathbf{d}^{cyc} \\ \mathbf{d}^{mist} \end{bmatrix} = \mathbf{b}, \tag{13}$$

where the matrices $\mathbf{A}_c$ and $\mathbf{A}_s$ are comprised of reorganized versions of $\mathbf{a}_{c1}$ and $\mathbf{a}_{c2}$ and of $\mathbf{a}_{s1}$ and $\mathbf{a}_{s2}$, respectively; $\mathbf{d}^{cyc} = \text{diag}\left[\boldsymbol{\Lambda}^{s^{-1}} \boldsymbol{\Lambda}^{\delta,s}\right]$ is the vector of cyclic modeling error values to be identified; and $\mathbf{d}^{mist} = \text{diag}\left[\boldsymbol{\Lambda}^{cb^{-1}} \boldsymbol{\Lambda}^{\delta,cb}\right]$ is the vector of blade mistuning values to be identified. Note that the cyclic modeling error and mistuning values are normalized by tuned system and cantilevered blade eigenvalues, respectively.

B. Selection Ratio (SR)

The CMM approach to mistuning identification presented in the previous section assumes that the system modes have certain properties typically present in blisks in frequency ranges with high modal density and blade-dominated motion. Therefore, a parameter called the selection ratio is introduced here to categorize modes according to how closely they match the assumptions and thereby how well they model the system.

One assumption is that the blade motion in the system modes of interest can be represented using a linear combination of cantilevered blade modes, that is $\boldsymbol{\Phi}^s = \boldsymbol{\Phi}^{cb} \mathbf{q}$. In order to check this assumption, the participation of the cantilevered blade normal mode(s) in the current system normal mode is computed. The participation factor with respect to the stiffness matrix for each blade in the system forms the matrix

$$\mathbf{q}_{\Phi}^{cb} = (\mathbf{F} \otimes \mathbf{I}) \underset{h=1,\ldots,P}{\tilde{\mathbf{B}}\mathbf{diag}} \left[\tilde{\mathbf{q}}_h^{cb}\right], \tag{14}$$

where $\underset{h=1,\ldots,P}{\tilde{\mathbf{B}}\mathbf{diag}}[\cdot]$ indicates a pseudo-block diagonal matrix, $\mathbf{F}$ denotes the real-valued Fourier matrix, and

$$\tilde{\mathbf{q}}_h^{cb} = \left[\boldsymbol{\Lambda}^{cb}\right]^{-1} \left(\boldsymbol{\Phi}^{cb^T} \mathbf{K}^{cb} \boldsymbol{\Phi}^s\right) \tag{15}$$

is the participation of the cantilevered blade normal modes in the cyclic system normal mode for harmonic h.[7] The matrix $\boldsymbol{\Lambda}^{cb}$ contains the cantilevered blade eigenvalues and the matrix $\mathbf{K}^{cb}$ is the stiffness matrix for the cantilevered blade. Large participation factors for each blade indicate that the motion of the blade in the system normal mode is well represented by the motion of the cantilevered blade normal mode and would be an advantageous choice to use in the ROM for the mistuning problem.

A second assumption in the CMM formulation of the mistuning identification problem is that the displacements at the interface between the blade and the disk are small for the system modes used in the ROM. These displacements can be written as $\boldsymbol{\Phi}^{s,\Gamma}$, where Γ denotes the boundary between the blades and the disk. If this motion is small relative to the motion of the blades for a given system normal mode, then this mode is a favorable choice for the IROM used for mistuning identification.

Using these two assumptions, a new criterion is formed to effectively evaluate the candidate system normal modes for the IROM used for mistuning identification. This criterion, called the Selection Ratio (SR), is defined as

$$SR_j = \frac{\|\mathbf{q}_{\Phi,j}^{cb}\|}{\|\boldsymbol{\Phi}_j^{s,\Gamma}\|}, \tag{16}$$

where j denotes the j^{th} system normal mode. This parameter accounts for the two assumptions inherent to the CMM formulation of the mistuning identification problem that have been identified as important for the mistuning identification procedure. System normal modes with large SR values agree favorably with both

of the noted CMM assumptions and therefore would be good candidates for the IROM used for mistuning identification.

Although the SR was derived specifically for the CMM approach to mistuning identification, it has a more general interpretation as well. For solving the mistuning identification problem, which is an inverse problem, the ROM should ideally contain only modes that show sensitivity to mistuning. In other words, any mode of the tuned system that would not be changed much by the mistuning is not helpful for solving the mistuning identification problem. Now, consider that the numerator of the SR is related to how strongly a change in a cantilevered blade eigenvalue (i.e., mistuning) affects the system eigenvalue, and the denominator of the SR is related to the strength of the blade-to-disk (and thus blade-to-blade) coupling. Thus, the SR is essentially a mistuning-to-coupling ratio for each system mode. It has been shown by Hodges[28] that the degree of mode localization increases monotonically with an increase in the mistuning-to-coupling ratio. Therefore, the SR is a metric that provides a quantitative assessment of the sensitivity of each system mode to blade mistuning. It is believed that similar metrics could be used with other mistuning identification techniques.

C. Physical to Modal Transformation

The CMM approach to mistuning transforms the analysis from physical to modal coordinates in order to reduce the model size. In general, consider the transformation from physical coordinates $\mathbf{x}$ to modal coordinates $\mathbf{p}$ expressed as

$$\mathbf{x} = \mathbf{\Phi}^s \mathbf{p}. \tag{17}$$

In order to reduce the model size, the matrix of tuned normal mode shapes $\mathbf{\Phi}^s$ is truncated. Typically, this truncation simply depends upon the frequency range of interest. The physical coordinates and tuned normal mode shapes are known, and the modal coordinates must first be found from Eq. 17, which is a least squares problem (since $\mathbf{\Phi}^s$ is truncated).

Measuring very many points per blade is prohibitively expensive. Hence, the mistuning identification procedure is based on experimentally measuring the vibration at only a few points on each blade. These measurement points also correspond to the DOF kept in the modal matrix used for the entire procedure. In this work, the measurement points are chosen using the Effective Independent Distribution Vector (EIDV) procedure introduced by Penny *et al.*[29]. Using a selected basis of tuned system normal modes, the EIDV algorithm selects DOF from a candidate set that will result in the modes being most distinguishable. It has been shown that the mistuning pattern can be effectively identified using as few as one point per blade.[21] Such a restrictive limit on the number of measured points introduces additional restrictions on the modes that can be used in the IROM. To correctly solve for $\mathbf{p}$ using Eq. 17, the number of measured DOF on the structure must be greater than or equal to the number of tuned system normal modes. Otherwise, the modal matrix, $\mathbf{\Phi}^s$, with the reduced number of DOF is rank deficient and that can adversely affect the mistuning identification results.

It should be noted that the modal matrix may become rank deficient even when it has more measurement points than system normal modes, i.e., in cases where multiple system normal modes cannot be distinguished with the given set of measurement points. An example of such a situation occurs in the case when only one point per blade is measured and different tuned system normal modes having the same number of nodal diameters are kept in the IROM. In this case, only one point is not enough to distinguish the modes with the same nodal diameter content, and therefore the modal matrix is rank deficient. In such a case, more DOF per blade must be used to achieve a modal matrix with full rank.

D. Solution of Known Mistuned Eigenvalue Problem to Generate Numerical Results

Sections II.B and II.C discussed ways of evaluating tuned system normal modes that are used as a basis for the mistuning identification procedure. With experience, a modeler could choose an appropriate ROM for the mistuning identification problem. In order to increase robustness and reduce the modeling expertise required to build a ROM for performing mistuning identification, a procedure to automatically construct an appropriate IROM is presented next.

Consider Eq. 9. Lim[27] suggested that, if damping is small and measurements are taken at resonant frequencies, then $\mathbf{f}^s$ and γ can be set to zero. This results in

$$-\omega^2 \mathbf{p} + \left[\mathbf{\Lambda}^s + \mathbf{\Lambda}^{\delta,s} + \mathbf{q}^{\mathrm{T}} \mathbf{\Lambda}^{\delta,cb} \mathbf{q}\right] \mathbf{p} = \mathbf{0}, \tag{18}$$

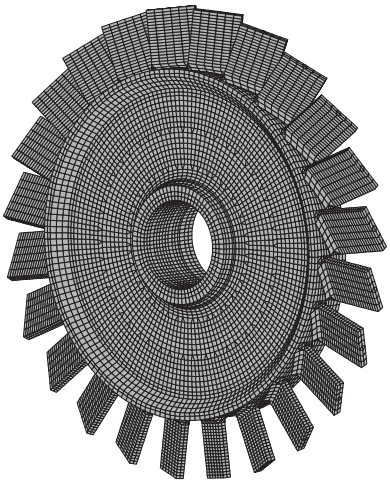

Figure 1. FEM of the blisk with 24 blades.

which can be viewed as an eigenvalue problem with ω as the eigenvalue and $\mathbf{p}$ as the eigenvector.

Here, it is suggested to first generate a blade stiffness mistuning pattern, $\mathbf{\Lambda}^{\delta,cb}_{gen}$, and the cyclic model updating pattern, $\mathbf{\Lambda}^{\delta,s}_{gen}$. (In this discussion, the normalization of the eigenvalue changes by the nominal eigenvalues has been dropped for convenience.) At this point, the eigenvalue problem is solved for $\mathbf{p}$ using the generated mistuning pattern, $\mathbf{\Lambda}^{\delta,cb}_{gen}$ and $\mathbf{\Lambda}^{\delta,s}_{gen}$. Note that the values of $\mathbf{p}$ must be perturbed in order to avoid a trivial solution where any IROM will give accurate results for the mistuning parameters. The solutions, ω and $\mathbf{p}$, are then used as surrogate data in Eq. 18 (inverse problem) where the blade stiffness mistuning, $\mathbf{\Lambda}^{\delta,cb}$, and the cyclic model updating, $\mathbf{\Lambda}^{\delta,s}$, are no longer considered known. This formulation represents the typical mistuning identification (inverse) problem, which can be solved for the mistuning parameters denoted by $\mathbf{\Lambda}^{\delta,cb}_{id}$ and $\mathbf{\Lambda}^{\delta,s}_{id}$. Of course, an exact identification gives $\mathbf{\Lambda}^{\delta,cb}_{id} = \mathbf{\Lambda}^{\delta,cb}_{gen}$ and $\mathbf{\Lambda}^{\delta,s}_{id} = \mathbf{\Lambda}^{\delta,s}_{gen}$. Here, *gen* stands for generated mistuning parameters that are used to solve the direct problem, and *id* stands for the mistuning parameters identified in the inverse procedure.

With perturbed values of $\mathbf{p}$, different IROMs can be evaluated by comparing the generated mistuning parameters with those solved by the mistuning identification procedure. By generating a mistuning pattern and solving for surrogate measurement data as suggested above, a mistuning pattern can be identified using the IROM. An error can be associated with the difference between the known and the identified values as $\| \mathbf{\Lambda}^{\delta,cb}_{gen} - \mathbf{\Lambda}^{\delta,cb}_{id} \|_2$ and $\| \mathbf{\Lambda}^{\delta,s}_{gen} - \mathbf{\Lambda}^{\delta,s}_{id} \|_2$ for the blade stiffness mistuning and the cyclic modeling error. Using these error metrics, the effectiveness of various IROMs for identifying mistuning parameters can be evaluated.

III. Effect of IROM on Mistuning Parameter Identification

It is not necessarily simple to select the best IROM for the identification of mistuning parameters. Certain modes are less compatible with the assumptions made in the CMM formulation of the mistuning identification procedure. As mentioned in Section II, a method of evaluating the suitability of various modes for the IROM has been developed. Also, the limited number of measurement points used for obtaining forced response data (which also corresponds to the DOF used to represent the tuned system normal modes in the IROM) has a significant impact on which modes should be selected for the mistuning identification procedure.

In this work, we use a 24-bladed disk (shown in Fig. 1) for validations. Only the first flexural bending mode of the cantilevered blade is used in the mistuning procedure. The candidate tuned system normal modes come from the 0-5000 Hz frequency range, which envelopes the first flexural blade mode family, as can be seen in the frequency versus nodal diameter plot in Fig. 2. The surrogate measurement data used in this section is comprised of the vibration response measured at each system resonance for a given frequency sweep. The surrogate measurement data is generated numerically using single-point harmonic excitation applied at blade 1.

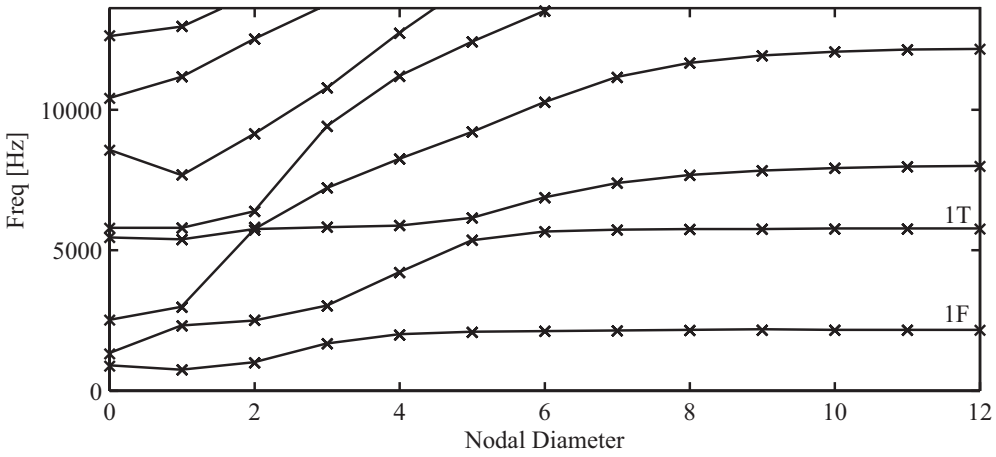

Figure 2. Natural frequencies versus nodal diameters for the blisk.

A. Selection Ratio

In Section II, the SR was presented to evaluate the tuned system normal modes that are candidates for the IROM used for mistuning identification. Using a sector of the FEM, the tuned system normal modes are computed in cyclic coordinates. Using only these modes, the SR values are computed for each mode. The modes are then ranked according to their SR values, with the highest SR value corresponding to most favorable mode. Thus, IROMs of increasing size can be constructed using this mode ordering. That is, at each iteration, the tuned system normal mode with the highest available SR value is added to the IROM. Figure 3 shows the mode shapes in the frequency range from 0 to 5000 Hz, which are most closely related to the first flexural cantilevered blade mode. It can be seen in Figs. 3a and 3b that the higher nodal diameter modes tend to have higher participation factors and smaller blade-disk interface motion. This indicates that these modes have more blade-dominant motion, whereas modes at lower nodal diameters (in the veering region) have significant disk motion. The blade-dominant modes typically have the largest SR values. These SR values are shown in Fig. 3c where the size of each circle denotes the SR value, and the numbers indicate the SR-based mode ordering.

Figure 4 depicts the information in Fig. 3c in a way that more clearly shows the SR values. In particular, the modes with low SR values, below the dotted line at SR value of 0.1, should not be used for constructing the IROM for mistuning identification.

The importance of the IROM construction with respect to yielding accurate mistuning identication results can be seen in Figs. 5 and 6. The measurement data used was from the frequency range 0-5000 Hz. The results from the mistuning identification formulation presented in this work (denoted by MistID) are compared with values computed using ANSYS. Figure 5 shows the blade stiffness mistuning, $\mathbf{\Lambda}^{\delta,cb}$ and cyclic modeling error, $\mathbf{\Lambda}^{\delta,s}$, in the case where all of the modes in the 0 to 5000 Hz frequency range are used in the IROM. Figure 5a shows that the general pattern of mistuning is not captured. Similarly, the cyclic modeling error values shown in Fig. 5b exhibit extremely large errors compared to their exact value of 0.01.

Figure 6 shows the mistuning identification results using a model that contains only the 15 modes that have SR values above the threshold value of 0.1 (see Fig. 4). It is clear that the results for both blade stiffness mistuning shown in Fig. 6a and cyclic modeling error shown in Fig. 6b have improved significantly from those shown in Fig. 5. These results indicate that the automatic mode selection based on SR values performed well in this case.

It should also be noted that the SR values provide useful information about the tuned system modes in general. Under the assumption that the blade motion in the system modes of interest can be represented using a cantilevered blade mode or combination of a few modes, one can determine to which family of blade modes the system mode belongs. In Fig. 3a, the cantilevered blade mode used to compute the participation factors was the first flexural blade mode. Therefore, the modes that belong to the first flexural blade mode

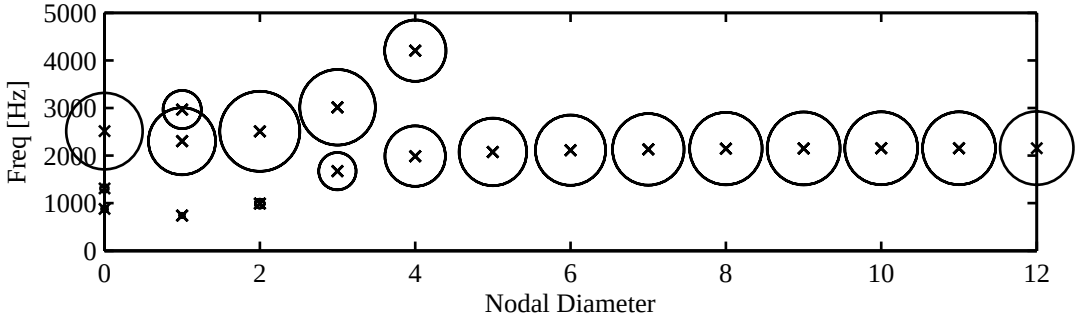

(a) Participation factors.

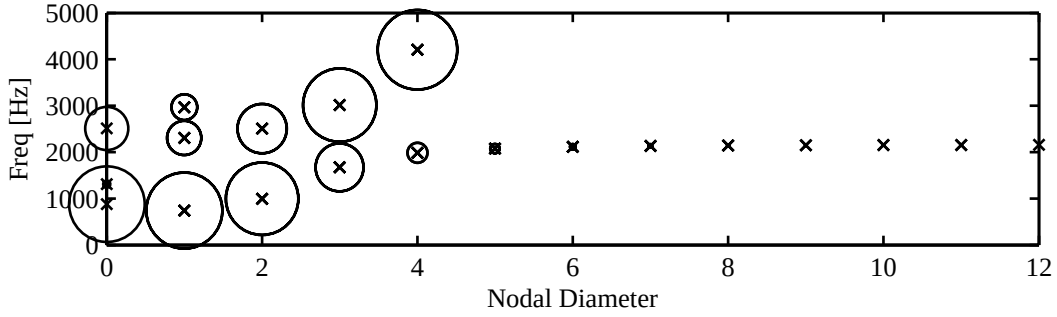

(b) Interface motion factors.

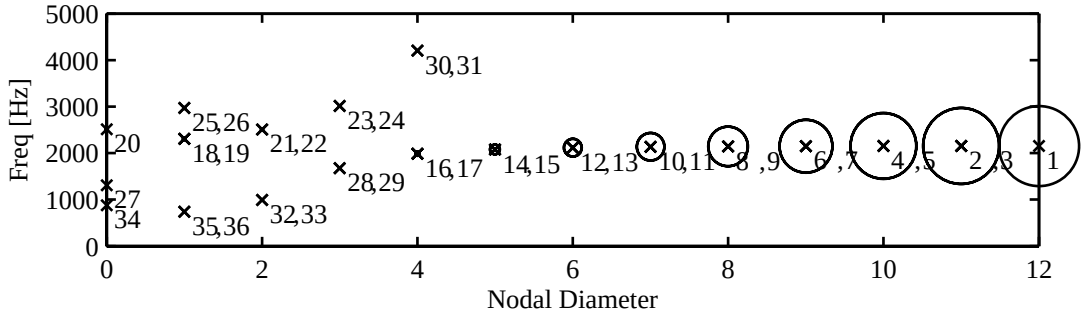

(c) Selection ratio (SR) factors. Numbers denote the mode selection order.

Figure 3. Parameters for IROM selection. The diameter of each circle indicates the magnitude of the parameter.

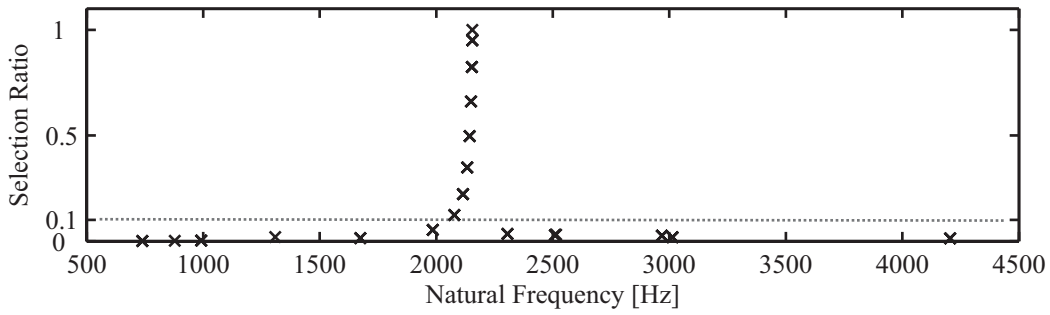

Figure 4. SR values versus natural frequency.

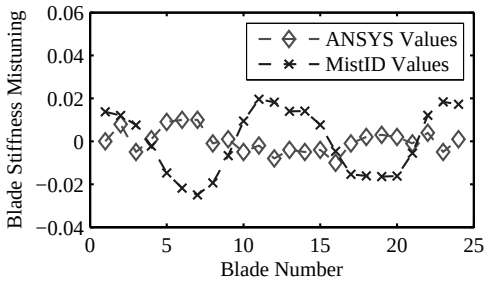

(a) Blade Stiffness Mistuning.

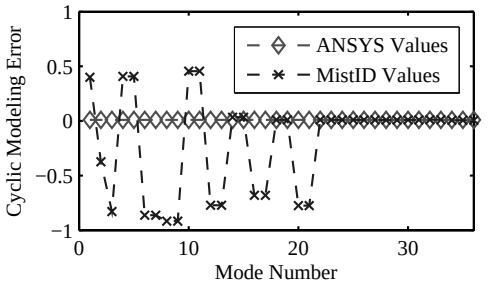

(b) Cyclic Modeling Error.

Figure 5. Identification results using a 36-DOF IROM (all modes in 0-5000 Hz).

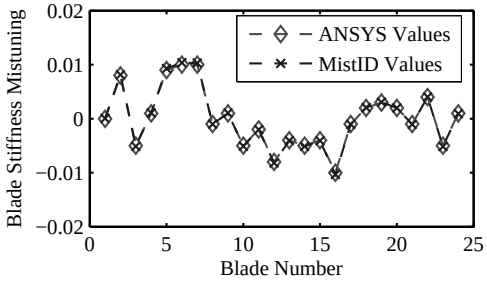

(a) Blade Stiffness Mistuning.

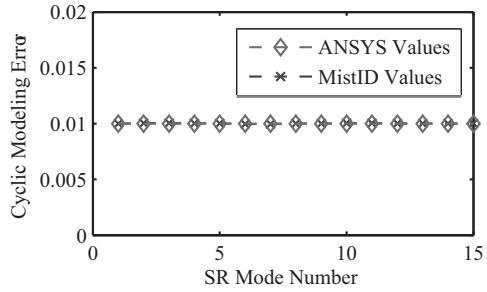

(b) Cyclic Modeling Error.

Figure 6. Identification results using a 15-DOF IROM (modes in 0-5000 Hz with SR value above 0.1).

family are shown by larger circles in Fig. 3c. The interface motion in Fig. 3b helps to adjust the selection ratio to show modes that most closely fit in that blade mode family.

B. Restriction on Nodal Diameter Representation based on a Limited Measurement Points

One key consideration while choosing the IROM for mistuning identification is the rank of the modal matrix containing the tuned system normal modes. This matrix can be rank deficient because only DOF physically measured on the structure are used to represent the mode shapes. For example, the matrix can become rank deficient when trying to distinguish between modes having the same nodal diameter when too few measurement points are used.

Figure 7 depicts the selection order of the mode shapes represented using only one measurement point per blade contained in the 1900-5000 Hz frequency range. The ordering of these modes is based strictly upon the SR values. It should be noted that the 23^{rd} and 24^{th} modes are the second mode pair added for the first nodal diameter. However, it is not until the 25^{th} and 26^{th} modes that the third nodal diameter is represented.

The rank of the modal matrix, given one measurement DOF per blade, is tracked in Fig. 9a as it is built up using the mode shapes ordered as shown in Fig. 7. Upon addition of the 23^{rd} mode to the IROM, the modal matrix becomes rank deficient. However, in Fig. 9b, where two measurement DOF per blade are used, the modal matrix does not become rank deficient.

In contrast to Fig. 7, the plot in Fig. 8 shows the ordering of the tuned system normal modes based upon the SR values with the exception of modes that would cause duplicity of the mode or mode pair for a given nodal diameter. Any mode or mode pair that would be the second for a given nodal diameter is not added until each nodal diameter has been represented by a mode or mode pair. As opposed to the ordering in Fig. 7, the ordering in Fig. 8 for the 23^{rd} and 24^{th} modes has changed to be at nodal diameter 3, which was previously only represented with the 25^{th} and 26^{th} modes.

The benefit of this selection procedure is that with one measurement point per blade (24 total measurement points), modes with differing nodal diameter content are far more distinguishable, and therefore will not result in a rank deficient matrix. This is shown in Fig. 10a where it is clear that the rank deficiency

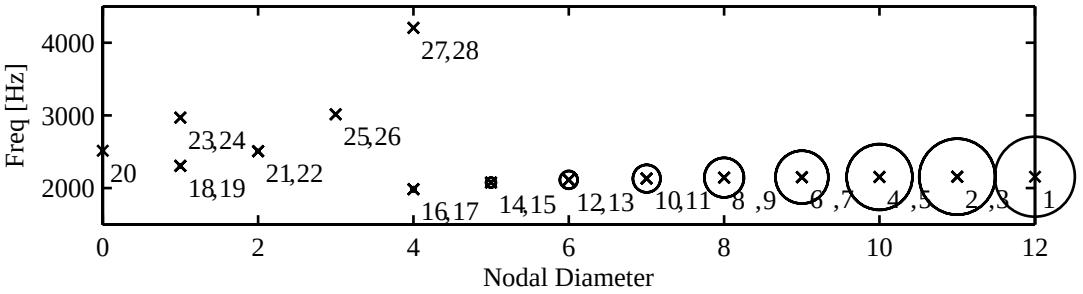

Figure 7. Mode ordering based strictly on SR values.

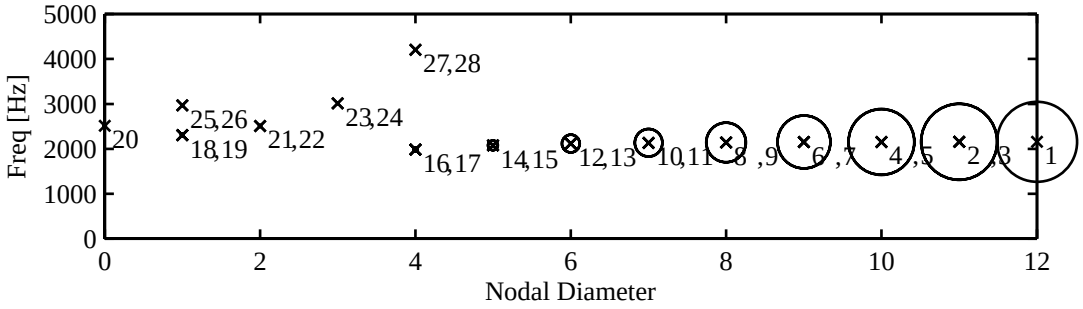

Figure 8. Mode ordering based on both SR values and nodal diameter content.

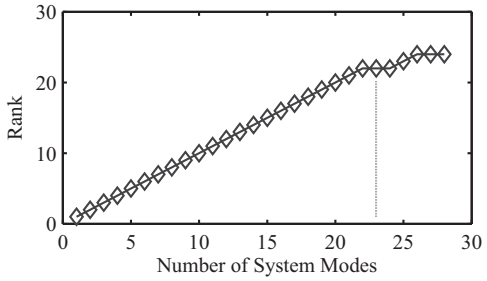

(a) One measurement DOF per blade.

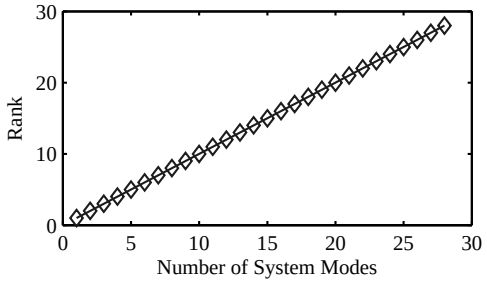

(b) Two measurement DOF per blade.

Figure 9. Rank of the modal matrix as the IROM is built up by adding modes based strictly on the SR values.

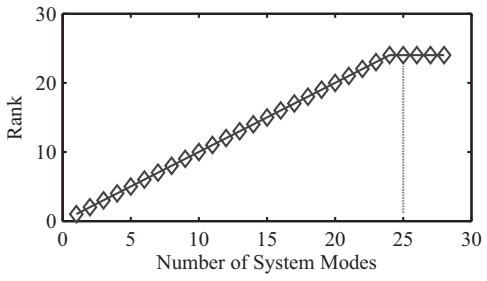

(a) One measurement DOF per blade.

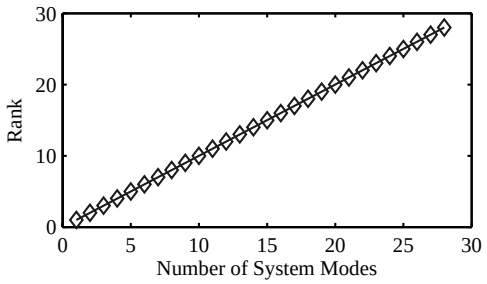

(b) Two measurement DOF per blade.

Figure 10. Rank of the modal matrix as the IROM is built up by adding modes based on both the SR values and nodal diameter content.

occurs at mode 25 which is the first mode added that duplicates a nodal diameter. Using the algorithm that ensures that all nodal diameter content is represented before duplicating nodal diameter modal content is recommended because of the limited number of DOF used to represent the mode shape. It can be seen in Fig. 10b that using a second measurement DOF per blade generates a modal matrix with full rank. In general, the restriction of nodal diameter content of modes can be eliminated by measuring more DOFs per blade than the number of modes or mode pairs of a given nodal diameter that will be used in the IROM.

IV. Evaluation of the Inverse ROM by Prescribing Surrogate Data

The results in Sections III.A and III.B show that IROM selection can be improved using the ideas presented in Sections II.A-C. However, an arbitrary lower threshold value of 0.1 for the SR values was used to determine the size of the IROM. This requires experience to generate an input to the procedure. Following the analysis presented in Section II.D, a more systematic and automatic method for selecting the IROM size is further examined.

Figure 11 shows a flowchart of the procedure that makes use of the analysis of Section II.D. The first step involves generating (i.e., prescribing) a mistuning pattern. It would generally be advisable to select a random mistuning pattern that has roughly the same level of mistuning that is expected, in order to most effectively evaluate the IROMs used for mistuning identification. At this point, it is important to distinguish between a ROM used to solve the direct problem (direct ROM or DROM) and a ROM used to solve the inverse problem (inverse ROM or IROM). The accuracy of the DROM with respect to the parent FEM increases monotonically as modes are added. Therefore, a DROM constructed from all the available modes in a given frequency range can be used in place of the FEM for solving the direct problem and generating the test data for a prescribed mistuning pattern. In contrast, the accuracy of the IROM does not increase monotonically as modes are added due to the nature of the least squares approximations used in Eq. 17 and in the solution of the inverse identification problem.

The generated/prescribed mistuning pattern is then plugged into the DROM where all of the modes for a given frequency range are employed. The governing equation for the DROM can viewed as an eigenvalue problem where the eigenvalue is ω and the eigenvector is $\mathbf{p}$. Solving for the eigenvalue and eigenvector yields preliminary surrogate data. Before this data can be used as surrogate measurement data, the eigenvector is perturbed. This avoids the trivial solution when the inverse problem is solved. If the data generated is unperturbed, all possible IROMs will yield nearly the same results and the identified mistuning will match with the generated mistuning with negligible error. Once the noise is added, the surrogate test data set is formed of perturbed eigenvectors and unperturbed eigenvalues of the DROM. This surrogate data is then plugged into the IROM, where the mistuning parameters are unknown. The IROM is made of a subset of the modes used in the DROM. Using the IROM with the surrogate data, a mistuning pattern can be computed. This mistuning pattern can be compared to the generated/prescribed mistuning pattern using the error presented in Section II.D. After the error is evaluated, additional modes are added to the IROM and another mistuning pattern is generated. The new resulting error can be computed. If the error reaches a minimum or a satisfactory level, the IROM selection is complete. This IROM can then be trusted to identify mistuning from real measured data. In this manner, the performance of various IROMs can be evaluated quantitatively while working only within the reduced-order modeling framework, and the IROM construction procedure can be fully automated.

In this section, the frequency range for possible mode shapes is 0-5000 Hz. The frequency range for measurement data is 1900-2160 Hz. Figure 12 shows the absolute error of the identification results as system modes are added to the IROM, using the FEM with prescribed mistuning as reference. First, the benefit of using the SR-based ordering of the modes to be included in the IROM is clear, as both mistuning and cyclic modeling error have smaller absolute error when the SR-based ordering is used. The detailed view of the mistuning in Fig. 12a shows that the error is suitably low in the range of 15–24 modes. However, the goal is to be able to predict which IROM will produce low absolute error, without knowing the solution from a FEM.

Figure 13 shows the absolute error of the identification results as system modes are added to the IROM, using a larger DROM with prescribed mistuning as reference, following the procedure described earlier in this section. For the direct problem, a 36-DOF DROM was constructed by retaining all system modes in the frequency range 0–5000 Hz. The level of perturbation to the eigenvectors $\mathbf{p}$ to produce the surrogate data was $\pm 1\%$ of $\mathbf{p}$. From the plots in Fig. 13, it is evident that the general trends of absolute error can

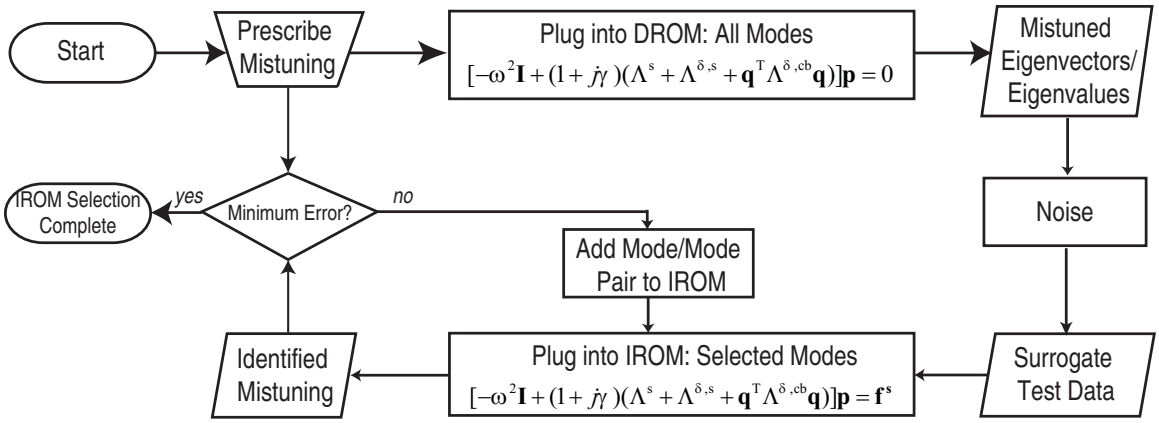

Figure 11. Flow chart for IROM evaluation using surrogate data.

be predicted by using a DROM with prescribed mistuning to generate surrogate test data. According to Fig. 13a, relatively low absolute error occurs for SR-ordered IROMs of size 13 through 19. Figure 14 shows the absolute errors for the direct problem, but with additional information about the blades. The sensitivity to modeling errors in the inverse problem is not uniform across all blades. So, it is possible for the error to be affected by the mistuning pattern. However, we observed that in general the error does not change significantly. This predicts that the selected IROM is a good choice for the mistuning identification procedure with respect to stiffness mistuning. Similar to the plot in Fig. 12b, Fig. 13b shows steadily increasing values of absolute error. Therefore, these results indicate that the error trends could be used to determine an IROM size that yields robust and accurate mistuning identification results.

V. Conclusions

Techniques to more effectively identify mistuning parameters of blisks using the CMM approach to mistuning were presented. A quantitative metric, the SR value, was introduced to systematically evaluate the tuned system modes used for forming the IROM in the CMM approach to mistuning identification. The SR values take into account the two assumptions made in the CMM technique, namely that the cantilevered blade normal mode shapes are similar to the blade portion tuned system normal mode shapes and that the blade-disk interface motion is small compared to the cantilevered blade motion. The SR values are generated using only information from the tuned system normal modes generated from the tuned FEM. Using these SR values, an effective IROM can be formed using tuned system normal modes. Using IROMs without ordering modes according to SR values can result in inaccurate mistuning identification. For these same cases, ordering modes according to the SR values leads to accurate mistuning parameters. Therefore, using this metric to select modes for the IROM can dramatically improve the accuracy of the mistuning identification results. It was also noted that these SR values could be used to categorize modes in a quantitative fashion according to blade mode families.

The effect of using a limited number of measurement points to represent the forced response and modes shapes was also considered. Because the current mistuning identification formulation is intended for use with experimental data, tuned system mode shapes are represented with a reduced number of DOF. This places a limitation on the number and type of tuned system modes that can be used in the IROM for mistuning identification. If there are not enough measurement points, the reduced modal matrix is rank deficient. An important example of such rank deficiency occurs when representing modes having the same nodal diameter content, as demonstrated in this paper. To use multiple modes with the same nodal diameter content, it was shown to be necessary to use more measurement DOF per blade than the number of modes (in the ROM) which have the same nodal diameter.

In addition, a novel technique has been developed to determine automatically a suitable IROM size for solving the mistuning identification inverse problem. The approach is to prescribe a blade mistuning pattern and compute surrogate measurement data numerically using a larger ROM for the direct problem. This measurement data is produced by solving the forward problem and then perturbing the solution before

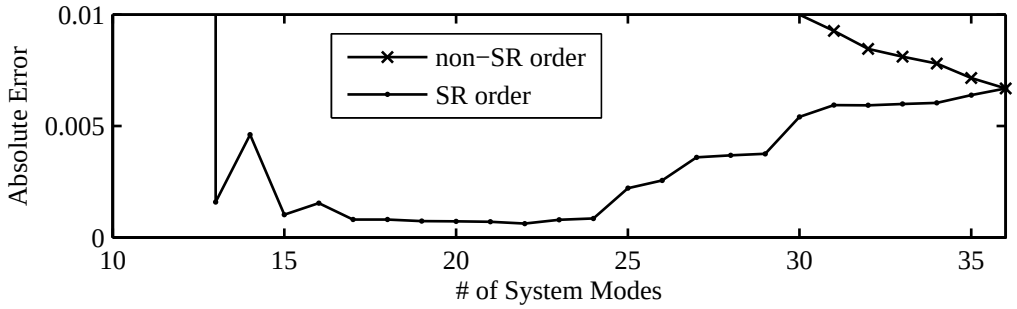

(a) Absolute Error of Blade Stiffness Mistuning.

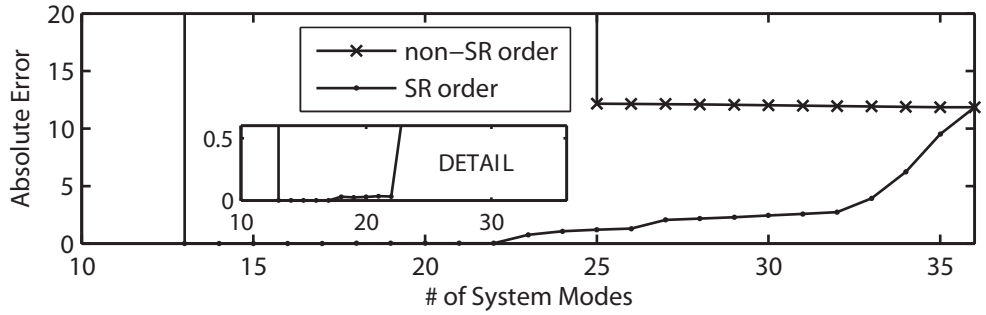

(b) Absolute Error of Cyclic Modeling Error.

Figure 12. Absolute error of the identification results as system modes are added to the IROM, using the FEM with prescribed mistuning as reference.

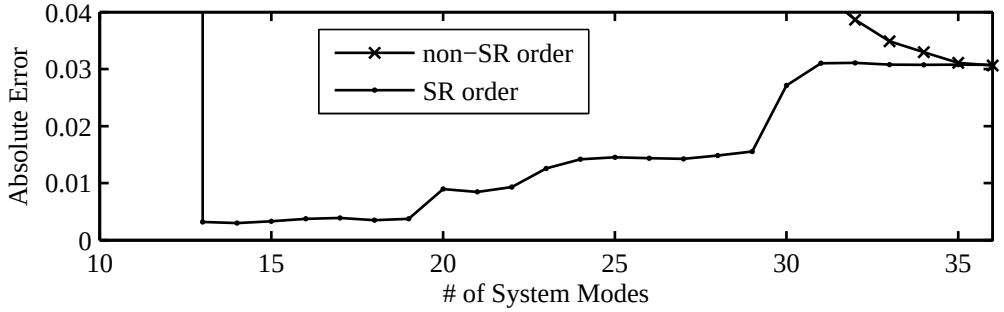

(a) Absolute Error of Blade Stiffness Mistuning.

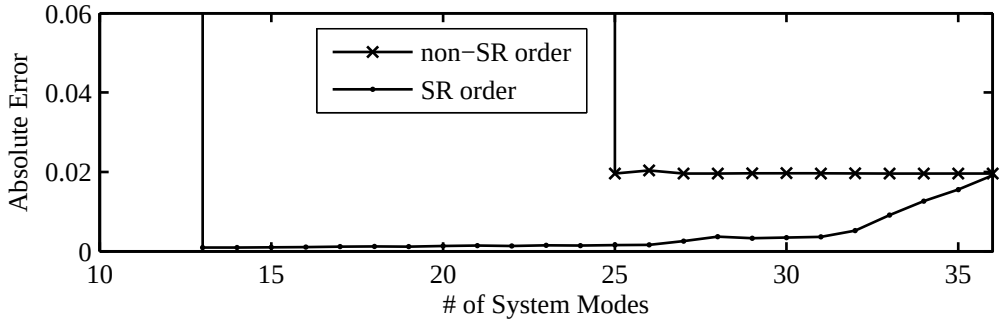

(b) Absolute Error of Cyclic Modeling Error.

Figure 13. Absolute error of the identification results as system modes are added to the IROM, using a DROM with prescribed mistuning as reference.

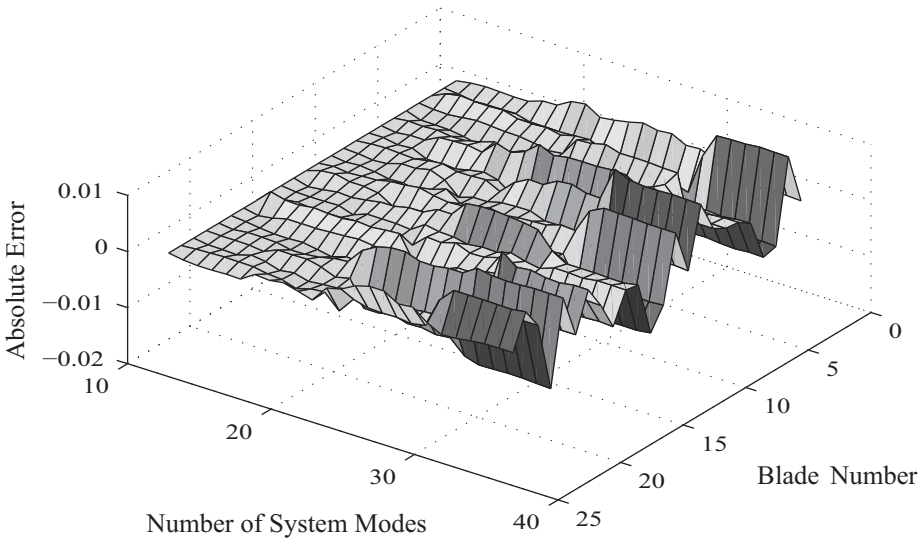

Figure 14. Absolute error of blade stiffness mistuning across all 24 blades.

plugging it into the inverse solver. The inverse formulation assumes that the mistuning is unknown and the IROM used is a subset of the ROM used for the direct problem. The solution to the inverse problem can then be compared directly to the prescribed mistuning pattern in order to check the performance of the IROM as modes are added. The results presented show that this process enables the automated construction of an IROM, and thus improve the overall accuracy and robustness of the mistuning identification. Furthermore, the automation of the procedure guarantees a systematic identification that does not demand the expertise that other current procedures require.

Acknowledgments

This work was supported by GE Aviation through the University Strategic Alliance (USA) program, with Dave Wisler as the program manager and Steve Manwaring and Sergio Filippi as the technical contacts. The authors would especially like to thank Sergio Filippi for many fruitful discussions and his helpful suggestions regarding this research. In this paper, there is no data representative of an actual GE blisk.

References

[1]Thomson, D. E. and Griffin, J. T., "The National Turbine Engine High Cycle Fatigue Program," *Global Gas Turbine News*, Vol. 39, No. 1, 1999, pp. 14–17.

[2]Castanier, M. P., Óttarsson, G., and Pierre, C., "A Reduced-Order Modeling Technique for Mistuned Bladed Disks," *Journal of Vibration and Acoustics*, Vol. 119, No. 3, 1997, pp. 439–447.

[3]Bladh, R., Castanier, M. P., and Pierre, C., "Component-Mode-Based Reduced Order Modeling Techniques for Mistuned Bladed Disks—Part I:Theoretical Models," *Journal of Engineering for Gas Turbines and Power*, Vol. 123, No. 1, 2001, pp. 89–99.

[4]Bladh, R., Castanier, M. P., and Pierre, C., "Component-Mode-Based Reduced Order Modeling Techniques for Mistuned Bladed Disks—Part II: Application," *Journal of Engineering for Gas Turbines and Power*, Vol. 123, No. 1, 2001, pp. 100–108.

[5]Yang, M.-T. and Griffin, J. H., "A Reduced-Order Model of Mistuning Using A Subset of Nominal System Modes," *Journal of Engineering for Gas Turbines and Power*, Vol. 123, No. 4, 2001, pp. 893–900.

[6]Feiner, D. M. and Griffin, J. H., "A Fundamental Model of Mistuning for a Single Family of Modes," *Journal of Turbomachinery*, Vol. 124, No. 4, 2002, pp. 597–605.

[7]Lim, S., Bladh, R., Castanier, M. P., and Pierre, C., "A Compact, Generalized Component Mode Mistuning Representation for Modeling Bladed Disk Vibration," *Collection of Technical Papers — AIAA/ASME/ASCE/AHS/ASC Structures, Structural Dynamics and Materials Conference*, Vol. 2, AIAA, Reston, VA, 2003, pp. 1359–1380.

[8]Lim, S., Bladh, R., Castanier, M. P., and Pierre, C., "Compact, Generalized Component Mode Mistuning Representation

for Modeling Bladed Disk Vibration," *AIAA Journal*, Vol. 45, No. 9, 2007, pp. 2285–2298.

[9]Mignolet, M. P. and Lin, C.-C., "Identification of Structural Parameters in Mistuned Bladed Disks," *Journal of Vibration and Acoustics*, Vol. 119, No. 3, 1997, pp. 428–438.

[10]Pichot, F., Thouverez, F., Jezequel, L., and Seinturier, E., "Mistuning Parameters Identification of a Bladed Disk," *Key Engineering Materials*, Vol. 204-205, 2001, pp. 123–132.

[11]Judge, J., Pierre, C., and Ceccio, S. L., "Experimental Identification of Mistuning in Blisks," *Proceedings of the 6th National Turbine Engine High Cycle Fatigue Conference*, Universal Technology Corporation, Dayton, OH, 2001.

[12]Judge, J., Pierre, C., and Ceccio, S. L., "Experimental Validation of Mistuning Identification Techniques and Vibration Predictions in Bladed Disks," *Proceedings of the International Forum on Aeroelasticity and Structural Dynamics*, Madrid, Spain, 2001.

[13]Judge, J. A., Pierre, C., and Ceccio, S. L., "Mistuning Identification in Bladed Disks," *Proceedings of the International Conference on Structural Dynamics Modelling*, Madeira, Portugal, 2002.

[14]Pierre, C., Judge, J., Ceccio, S. L., and Castanier, M. P., "Experimental Investigation of the Effects of Random and Intentional Mistuning on the Vibration of Bladed Disks," *Proceedings of the 7th National Turbine Engine High Cycle Fatigue Conference*, Universal Technology Corporation, Dayton, OH, 2002.

[15]Feiner, D. M. and Griffin, J., "A Completely Experimental Method of Mistuning Identification in Integrally Bladed Rotors," *Proceedings of the 8th National Turbine Engine High Cycle Fatigue Conference*, Universal Technology Corporation, Dayton, OH, 2003, pp. 1–1–1–13.

[16]Kim, N. E. and Griffin, J., "System Identification in Higher Modal Density Regions of Bladed Disks," *Proceedings of the 8th National Turbine Engine High Cycle Fatigue Conference*, Universal Technology Corporation, Dayton, OH, 2003, pp. 1–68–1–82.

[17]Feiner, D. and Griffin, J., "Mistuning Identification of Bladed Disks Using a Fundamental Mistuning Model—Part I: Theory," *Journal of Turbomachinery*, Vol. 126, No. 1, 2004, pp. 150–158.

[18]Feiner, D. and Griffin, J., "Mistuning Identification of Bladed Disks Using a Fundamental Mistuning Model—Part II: Application," *Journal of Turbomachinery*, Vol. 126, No. 1, 2004, pp. 159–165.

[19]Lim, S., Castanier, M. P., and Pierre, C., "Mistuning Identification and Reduced-Order Model Updating for Bladed Disks Based on a Component Mode Mistuning Technique," *Proceedings of the 9th National Turbine Engine High Cycle Fatigue Conference*, Universal Technology Corporation, Dayton, OH, 2004.

[20]Li, J., Pierre, C., and Ceccio, S. L., "Validation of a New Technique for Mistuning Identification and Model Updating Based on Experimental Results for an Advanced Bladed Disk Prototype," *Evaluation, Control and Prevention of High Cycle Fatigue in Gas Turbine Engines for Land, Sea and Air Vehicles (Meeting Proceedings RTO-MP-AVT-121)*, NATO Research and Technology Organisation, Neuilly-sur-Seine, France, 2005, pp. 36–1–36–16.

[21]Song, S. H., Castanier, M. P., and Pierre, C., "System Identification of Multistage Turbine Engine Rotors," *Proceedings of the ASME Turbo Expo 2007*, No. GT2007-28307, American Society of Mechanical Engineers, New York, 2007.

[22]Pichot, F., Laxalde, D., Sinou, J. J., Thouverez, F., and Lombard, J. P., "Mistuning identification for industrial blisks based on the best achievable eigenvector," *Computers & Structures*, Vol. 84, No. 29–30, 2006, pp. 2033–2049.

[23]Lim, T. W. and Kashangaki, T. A. L., "Structural damage detection of space truss structures using best achievable eigenvectors," *AIAA Journal*, Vol. 32, No. 5, 1994, pp. 1049–1057.

[24]Hurty, W. C., "Dynamic Analysis of Structural Systems Using Component Modes," *AIAA Journal*, Vol. 3, No. 4, 1965, pp. 678–685.

[25]Craig, Jr., R. R. and Bampton, M. C. C., "Coupling of Substructures for Dynamic Analyses," *AIAA Journal*, Vol. 6, No. 7, 1968, pp. 1313–1319.

[26]Yang, M.-T. and Griffin, J. H., "A Normalized Modal Eigenvalue Approach for Resolving Modal Interaction," *Journal of Engineering for Gas Turbines and Power*, Vol. 119, No. 3, 1997, pp. 647–650.

[27]Lim, S.-H., *Dynamic Analysis and Design Strategies for Mistuned Bladed Disks*, Ph.D. thesis, The University of Michigan, Ann Arbor, April 2005.

[28]Hodges, C. H., "Confinement of Vibration by Structural Irregularity," *Journal of Sound and Vibration*, Vol. 82, No. 3, 1982, pp. 411–424.

[29]Penny, J. E. T., Friswell, M. I., and Garvey, S. D., "Automatic Choice of Measurement Locations for Dynamic Testing," *AIAA Journal*, Vol. 32, No. 2, 1994, pp. 407–414.